ISSN 1063-7710, Acoustical Physics, 2019, Vol. 65, No. 2, pp. 178–184. © Pleiades Publishing, Ltd., 2019.

PHYSICAL ACOUSTICS

Low-loss Floating Electrode Unidirectional Transducer for SAW Sensor[1]

J. X. Zhai[a] and C. Chen[a, *]

[a]*Optoelectronic Information Science and Technology Changchun University of Science and Technology, Changchun, 130022 China*

**e-mail: chen_chen_1982@163.com*

Received August 10, 2018; revised September 13, 2018; accepted October 30, 2018

Abstract—Two types of interdigital transducer (IDT) structures of SAW devices have been investigated; one type consists in a classical single electrode transducer where the unit cell has two electrodes, and the other type has a design of floating electrode unidirectional transducer (FEUDT) where the unit cell has six electrodes per period. By taking the Fourier transform of the corresponding time response, the insertion loss (IL) of the SAW device with FEUDT is calculated as –2.6 (forward) and –20.5 dB (backward). At the same time, the device with conventional IDT exhibits an IL value of –8.4 (forward) and –7.8 dB (backward). It turns out that the design of a novel FEUDT type SAW device can efficiently reduce the insertion loss of the SAW device.

Keywords: floating electrode, unidirectional transducer, insertion loss, bidirectional IDT, SAW sensor

DOI: 10.1134/S106377101902012X

1. INTRODUCTION

Recently, chemical sensors based on a surface acoustic wave (SAW) have been widely investigated due to several attractive advantages, such as high sensitivity, small size, reliability and wireless ability [1–9]. Figure 1 shows the most popular SAW sensor structure, which consists of transmitting interdigital transducer (IDT) and receiving IDT separated by delay line. The delay line is covered by a sensing film. The performance of such a SAW sensor using a conventional bidirectional transducer is degraded by the triple-transit echo, and the insertion loss (IL) is also increased by bidirectional propagation loss.

The unidirectional transducers (UDT) technique using reflections within the transducers can suppress the triple-transit echo and improve the IL owing to its inherent unidirectional directivity [10–12]. Various UDT structures, such as the distributed acoustic reflection transducer (DART) [13], electrode-width controlled (EWC) [14], Hunsinger-geometry SPUDT [15] have already been reported. Narrow gap floating electrode unidirectional SAW transducers (FEUDTs) were developed in 1984 by Yamanouchi [16] making use of the reflection from floating, i.e. electrically disconnected electrodes. The main advantages are higher operation frequencies for the same electrode width compared to conventional IDTs with a metallization (line-to-space) ratio of 1 : 1, a smaller electrode resistance due to the wider electrodes, and the efficient excitation of higher harmonics due to the larger metallization ratio.

In this paper, a novel SAW sensor using FEUDT is proposed to improve the characteristics of the SAW device. FEUDT is to enhance the generated signal in the forward direction, but reduce the signal in the reverse direction using the distributed reflection sources in the transducer. It can effectively minimize the IL compared to conventional bidirectional IDT.

2. THEORY DESCRIPTION

The piezoelectric constitutive relations, as Eqs. (1) and (2) express, completely describe the interplay of stress, strain, and electric field in a piezoelectric solid [17]:

$$T_{ij} = C^E_{ijkl} S_{kl} - e^T_{ijk} E_k, \quad (1)$$

$$D_i = e_{ikl} S_{kl} + \varepsilon^S_{ij} E_j, \quad (2)$$

where T_{ij} represents the stress vector; C^E_{ijkl} is the elasticity matrix (N/m^2); S_{kl} is the strain vector; e^T_{ijk} and e^S_{ij} are the piezoelectric stress matrixes (C/m^2), which represent the energy conversion between the electrical and mechanical fields; E_k is the electrical field vector (V/m); D_i is the electrical displacement (C/m^2); and ε^S_{ij} is the permittivity matrix (F/m). The subscripts i, j

[1] The article is published in the original.

and k represent the displacements of freedom in the x-, y- and z-directions, respectively. The superscript T indicates that e_{ijk} and e_{ikl} transpose each other. The superscript E on C_{ijkl}^{E} and S on ε_{ik}^{S} indicates that they are the properties at a constant electric field and strain, respectively.

Acoustic wave propagation in a piezoelectric substrate involves the coupling of the displacement and the electromagnetic fields. The equation of motion can be obtained by coupling with Maxwell's equations for the electromagnetic fields through the piezoelectric constitutive equations. The magnetic field is assumed static, and the electric field can be calculated as the negative gradient of the potential, as Eq. (3) shows [18]:

$$E_i = -\frac{\partial \phi}{\partial r_i}. \tag{3}$$

By substituting the equation of motion ($F = ma$) and Eq. (3) into Eq. (1), the piezoelectric constitutive relations can be written as Eq. (4) [18]:

$$C_{ijkl}^{E}\frac{\partial^2 u_k}{\partial r_j \partial r_l} + e_{ijk}^{T}\frac{\partial^2 \phi}{\partial r_k \partial r_j} = \rho\frac{\partial^2 u_i}{\partial t^2}, \tag{4}$$

where ρ is the area density (kg/m^2) and u is the displacement.

Since the general piezoelectric thin films have almost no conducting charges, the divergence of the electrical displacement can be regarded as zero, as Eq. (5) shows [18]:

$$\frac{\partial D_i}{\partial r_i} = e_{ikl}\frac{\partial^2 u_k}{\partial r_l \partial r_i} + \frac{\partial}{\partial r_i}\left(-\varepsilon_{ij}^{S}\frac{\partial \phi}{\partial r_j}\right) = 0. \tag{5}$$

Therefore, the wave equation of the SAW devices can be obtained as shown in Eq. (6) [18]:

$$e_{ikl}\frac{\partial^2 u_k}{\partial r_l \partial r_i} = \varepsilon_{ij}^{S}\frac{\partial^2 \phi}{\partial r_i \partial r_j}. \tag{6}$$

The displacements and the voltage of the SAW devices can be calculated by solving the wave equation. This paper utilizes a finite element method and the abovementioned wave equation to simulate the operating modes and the frequency response of the proposed SAW devices.

3. FEM MODEL DESCRIPTION

Two types of IDT structures (A and B) have been investigated in this research, and the results have been compared. Structure A (Fig. 2a) consists of a classical single electrode transducer, where the unit cell has two electrodes. Structure B (Fig. 2b) is a FEUDT, where

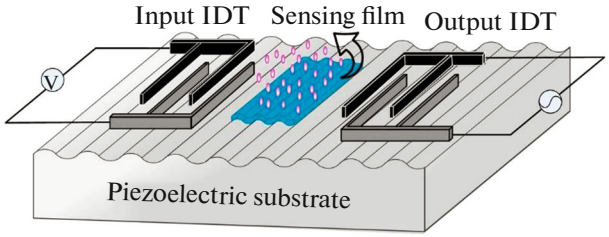

Fig. 1. SAW sensor structure.

the unit cell has six electrodes per period. Electrodes 1 and 4 are fixed on the bus bars and connected to the RF electrical power; electrodes 2, 3, 5 and 6 are floating, and electrodes 2 and 5 are connected to each other. The fixed electrodes and the connected floating electrodes play an important role in the excitation of the SAW, this makes the center of excitation away from the center of reflection, and the amplitude of the leftward SAW is not equal to the rightward one.

According to the SAW theory, the relationship between the period of IDT fingers (denoted as p), the wavelength of the surface propagation wave (denoted as Λ), and the central frequency (f_0) of the SAW device can be given by:

$$f_0 = \frac{V}{\lambda} = \frac{V}{2p}. \tag{7}$$

Once the piezoelectric thin film material is selected, the phase velocity v of the propagation wave is a constant, and thus the operation frequency of the SAW device can be determined by the IDT period designed. In this research, the piezoelectric material is 128° Y–X $LiNbO_3$ whose acoustic velocity is 4000 m/s. The expected center frequency of this SAW device is 200 MHz. To achieve that, the SAW wavelength at 24 μm is selected.

In order to model one wavelength of the SAW device, boundary conditions shown in Fig. 3 have to be added and defined. The right (Γ_R, Γ_R') and the left (Γ_L, Γ_L') vertical boundary conditions are defined as periodic ones for both bidirectional and FEUDT structures to have the same displacement and potential. The top boundary (Γ_2, Γ_2') is free [19], and bottom boundary (Γ_1, Γ_1') is fixed. The electrical boundary conditions include electrical inputs and the zero charge constraint. We set the electric potential for each active finger +1 and −1 V, respectively.

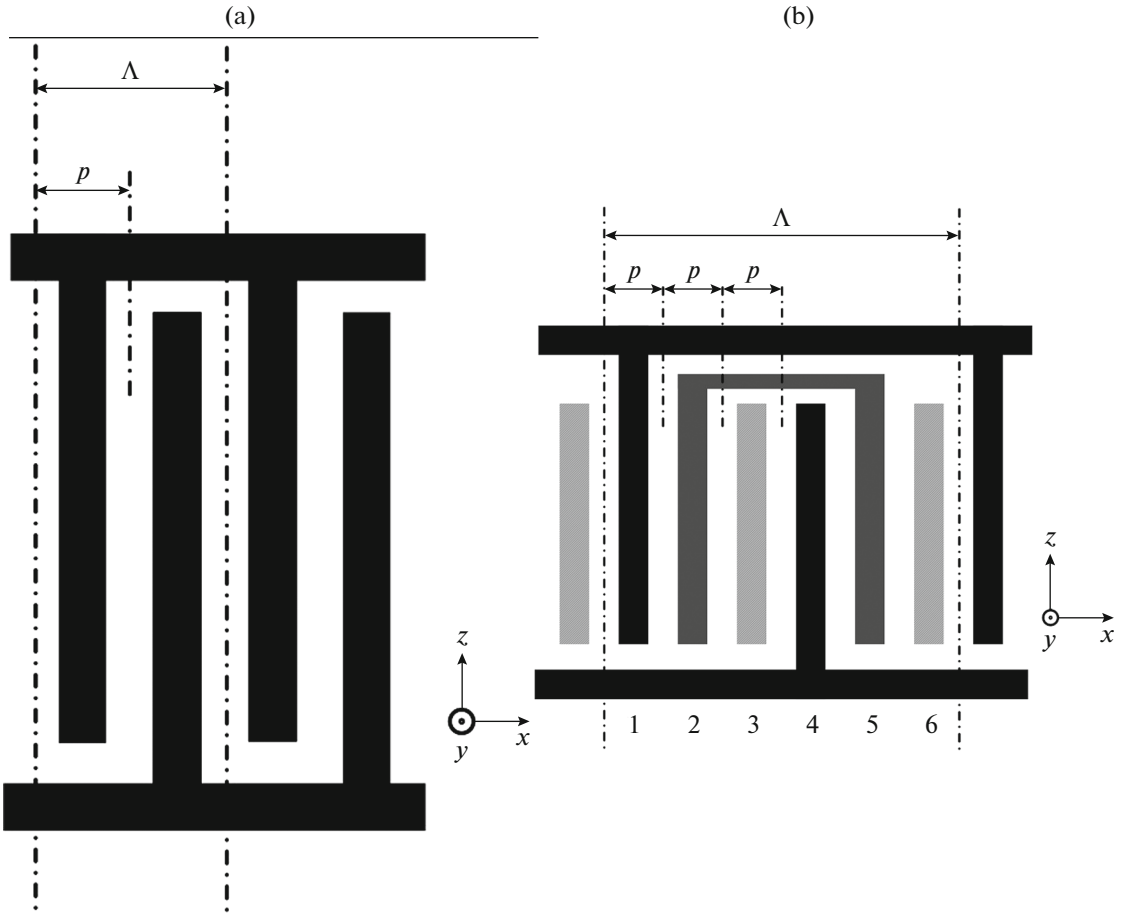

Fig. 2. (a) Bidirectional IDT and (b) FEUDT configurations of the SAW sensor.

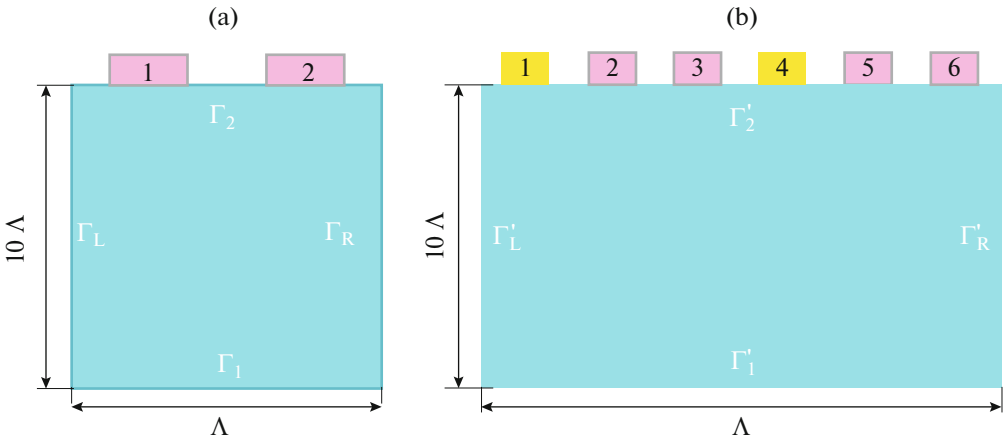

Fig. 3. 2D unit cell structure employed in the FEM simulation for (a) bidirectional and (b) FEUDT configurations.

4. SIMULATION RESULTS AND DISCUSSIONS

4.1. Eigenfrequency Analysis

Eigenfrequency analysis gives the modes of the structure and their corresponding frequencies. We use this study to identify fundamental modes and the working frequency range of the SAW device.

The SAW modes can be identified from the eigenvectors (mode shapes) displayed in Fig. 4. One of the

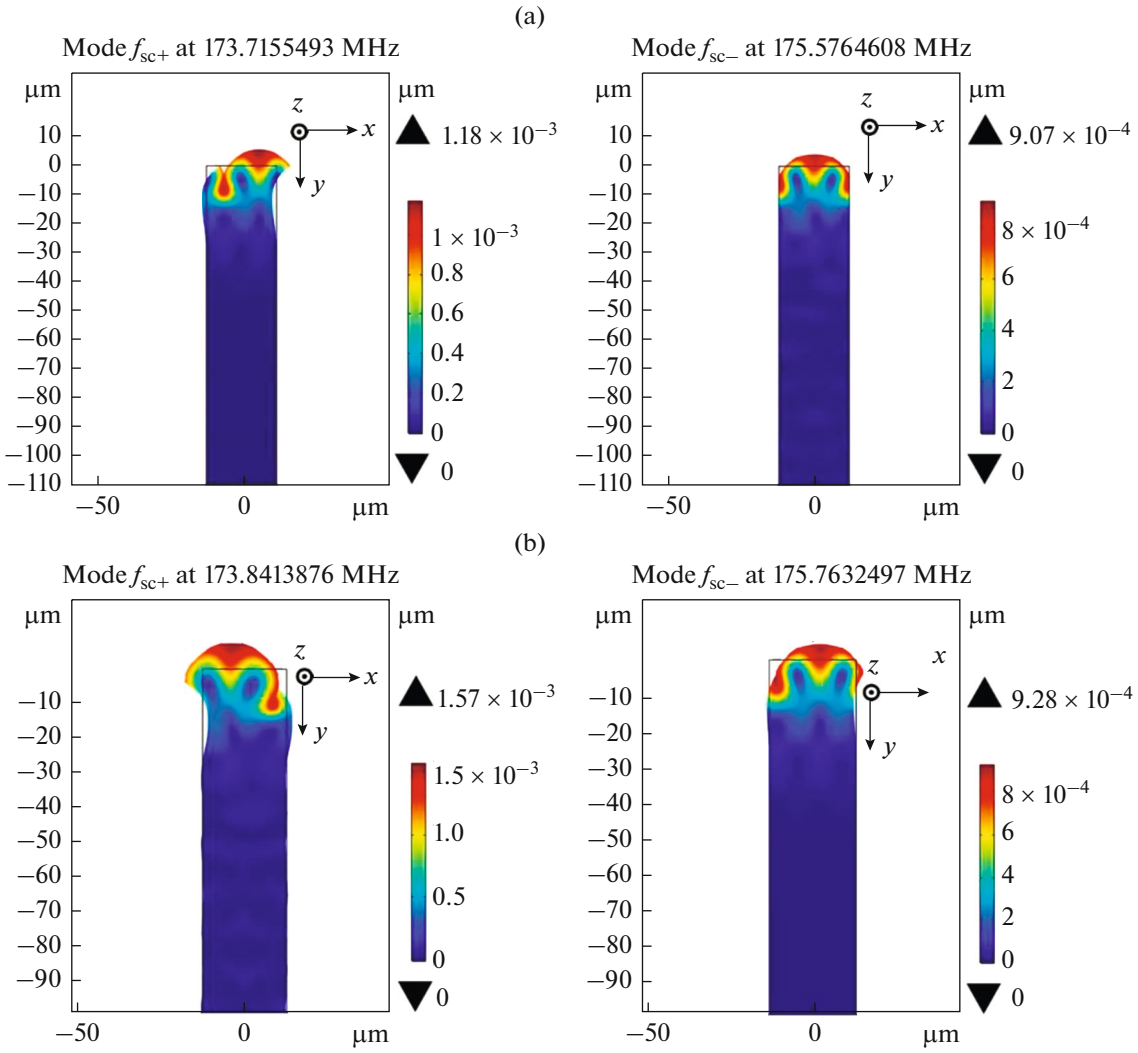

Fig. 4. SAW mode shapes: (a) for bidirectional IDT, (b) for FEUDT.

modes has zero displacement component in the X-direction (f_{sc-}) at both the ends and the other has zero displacement component in the Y-direction (f_{sc+}) at the ends. Two eigenfrequencies (f_{sc-} and f_{sc+}) are the edges of the stopband. There is no propagation into the media in this range of frequencies.

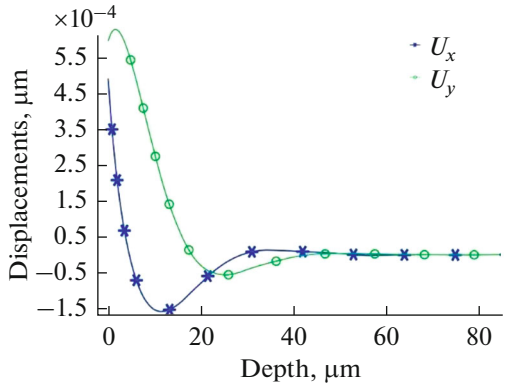

Fig. 5. SAW displacement profile for bidirectional IDT at resonant frequency.

The components of displacements U_x (in the propagation direction) and U_y (in the depth direction) plotted against the depth and propagation direction coordinates are shown in Figs. 5 and 6, respectively. Both the U_x and U_y die down within 2 to 3 wavelengths, as seen from Fig. 5; on the surface of the substrate, they are 90° out-of-phase with each other. These illustrate the important properties of Rayleigh mode of SAW. We can observe the similar distributions of the displacement fields for FEUDT, which are omitted here.

From Fig. 4, we can calculate the center frequencies, which are 174.65 and 174.80 MHz for bidirectional IDT and FEUDT respectively.

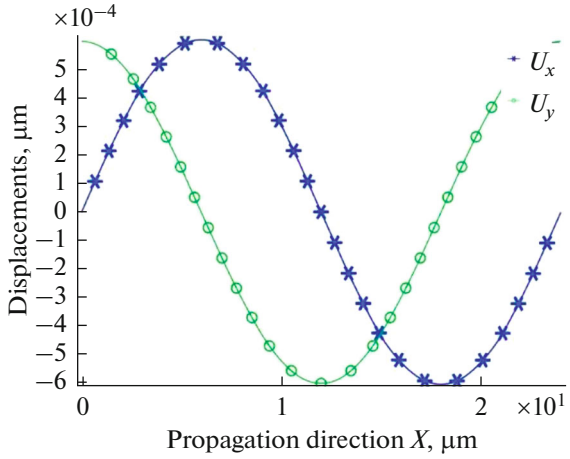

Fig. 6. Phase difference between U_x and U_y for bidirectional IDT.

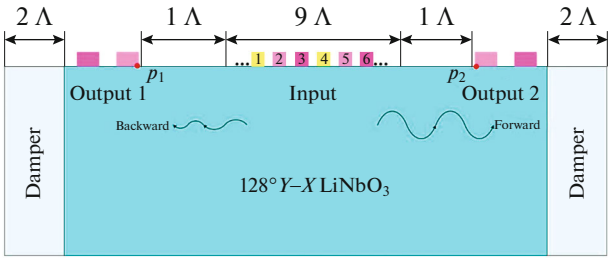

Fig. 7. Simulation geometry of the Rayleigh type SAW delay line.

4.2. Time Domain Analysis

The SAW delay line model considered for the simulation is shown in Fig. 7. In the simulation, a transmitting IDT consisting of nine periods (9Λ) and a delay line of 24 μm (Λ) is considered. Critical damping is assumed to the left of the input IDT (sub-domain "Damper") and right of the output IDT ("Damper" domain) to avoid reflections back to the delay line [20]. To analyze the SAW propagation over the delay line, transient analysis of the SAW delay line is performed with a time interval of 0.1 ns for 110 ns for 174 MHz and 2 V peak-to-peak (V_{in}) input sine wave.

The values of wave energy in forward and backward directions for FEUDT and bidirectional IDT are achieved from surface elements and presented in Figs. 8a and 8b, respectively. For bidirectional IDT, the wave energy in the forward direction is similar to that in the backward direction, which illustrates the bidirectional operation. However, for FEUDT, the SAW exhibits in the forward direction growing intensity profiles, and the acoustic energy is much greater, which demonstrates the strong unidirectional operation.

To compare the IL of the FEUDT to that of bidirectional IDT, a 2D structure model shown in Fig. 7 is used. The IL of the device is found by taking the Fourier transform of the time response. It is calculated by the relation [21]

$$\mathrm{IL(dB)} = 20\log\left(\left|V_{\mathrm{out}}/V_{\mathrm{in}}\right|\right). \qquad (8)$$

The output electric potentials V_{out} of the SAW are recorded at points p_1 and p_2. By utilizing the formula (8), the insertion losses of the SAW device with FEUDT is calculated as –2.6 (forward) and –20.5 dB (backward), respectively. The device with bidirectional IDT exhibits an IL value of –8.4 (forward) and –7.8 dB (backward). It turns out that the design of the FEUDT type SAW device can efficiently reduce the IL of the SAW device.

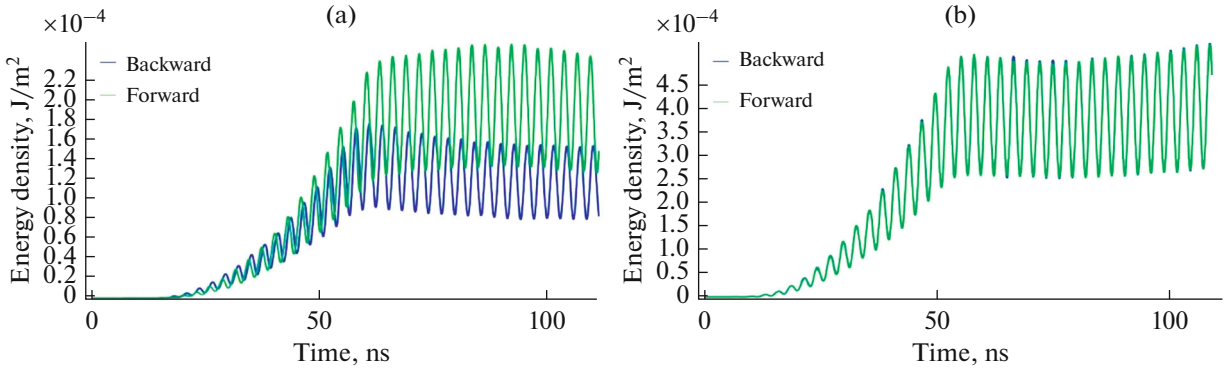

Fig. 8. Acoustic energies of forward and reverse directions: (a) FEUDT, (b) bidirectional IDT.

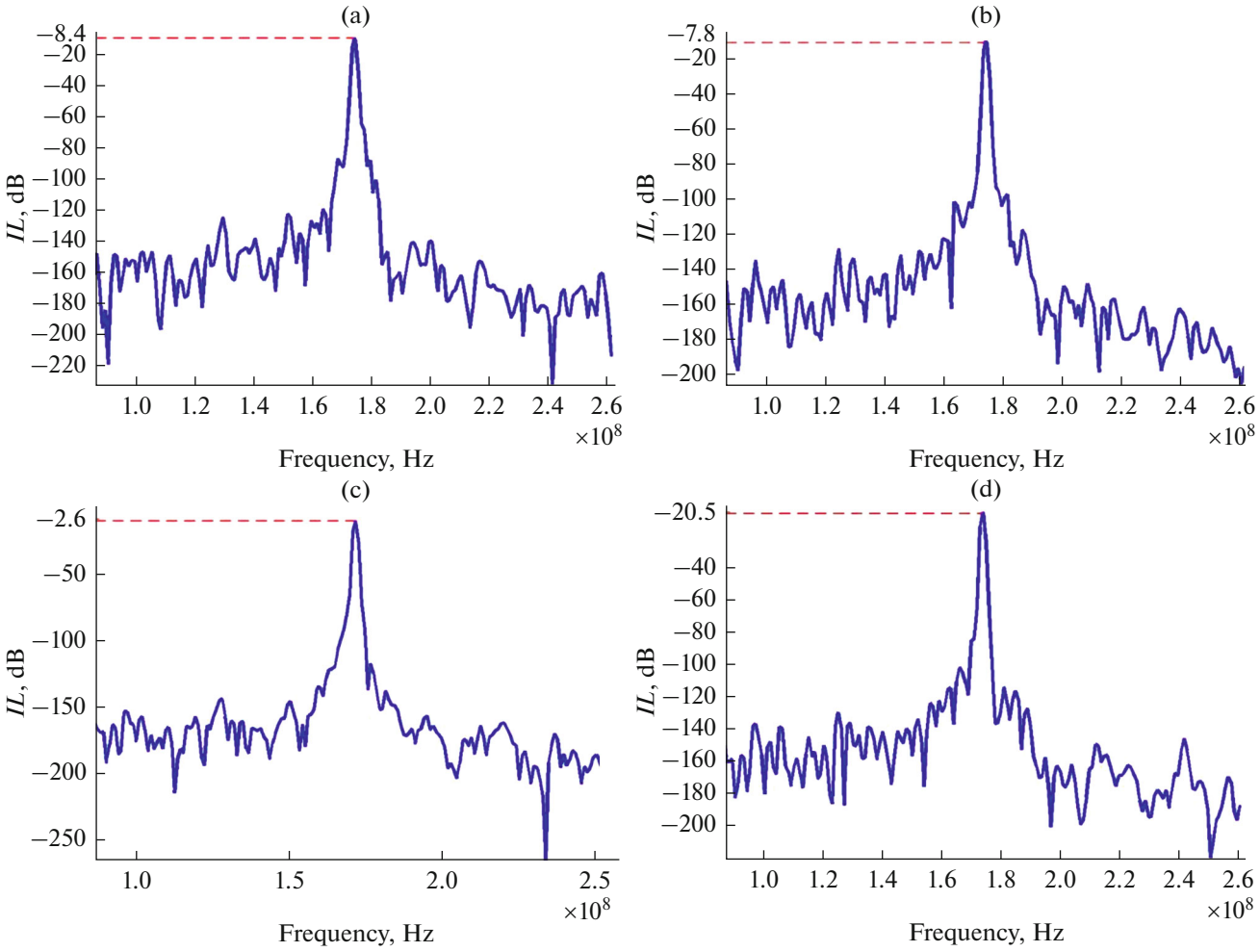

Fig. 9. Frequency response of the FEUDT and bidirectional IDT of forward and reverse direction: IL for bidirectional IDT (a) forward and (b) backward; IL for FEUDT (c) forward and (d) backward.

5. CONCLUSIONS

This paper focuses on minimizing the insertion loss of the IDT for the SAW sensor application. We perform the eigenfrequency study to identify fundamental modes that confirm the Rayleigh wave nature. By time domain analysis and Fourier transform of the corresponding time response, the higher acoustic energy (forward direction) and lower insertion loss are observed in FEUDT compared to a bidirectional IDT. Therefore, the novel FEUDT type SAW sensor has got our attention because of its potential ability to highly improve the sensitivity of the sensor.

ACKNOWLEDGMENTS

The authors gratefully acknowledge the National Natural Science Foundation of China for financial support of this work (Grant no. 11604025).

REFERENCES

1. A. Maskay and M. P. D. Cunha, Sens. Actuators, A **259**, 34 (2017).
2. N. Fourati and C. Zerrouki, in *Proc. 32nd General Assembly and Scientific Symposium of the Int. Union of Radio Science* (Montreal, 2017), p. 1.
3. D. B. Go, M. Z. Atashbar, Z. Ramshani, and H. C. Chang, Anal Methods **9**, 4112 (2017).
4. F. Zhang, H. Dong, X. Zhang, J. Guo, Y. Liu, C. Zhou, X. Zhang, J. Liu, M. Yan, and X. Chen, Anal. Sci. **33** (11), 1271 (2017).
5. R. Takpara, M. Duquennoy, M. Ouaftouh, C. Courtois, F. Jenot, and M. Rguiti, Res. Nondestr. Eval. (2016).
6. D. Sil, J. Hines, U. Udeoyo, and E. Borguet, ACS Appl. Mater. Interfaces, **7** (10), 5709 (2015).
7. H. S. Hong and G. S. Chung, Sens. Actuators, B **148** (2), 347 (2010).

8. M. Y. Dvoesherstov and V. I. Cherednik, Acoust. Phys. **61** (6), 657 (2015).
9. Y. Fan and X. Ji, Acoust. Phys. **64** (1), 122 (2018).
10. K. Hamma and B. J. Hunsinger, in *Proc. IEEE Ultrasonics Symposium* (1976), p. 328.
11. C. S. Hartmann, P. V. Wright, R. J. Kansy, and E. M. Garbe, in *Proc. IEEE Ultrasonics Symposium* (San Diego, CA, 1982), p. 40.
12. P. V. Wright, in *Proc. IEEE Ultrasonics Symposium* (San Francisco, CA, 1985), p. 58.
13. T. Kodama, H. Kawabata, Y. Yasuhara, and H. Sato, in *Proc. IEEE Ultrasonics Symposium* (Williamsburg, VA, 1986), p. 59.
14. C. S. Hartmann and B. P. Abbott, in *Proc. IEEE Ultrasonics Symposium* (Montreal, 1989), p. 79.
15. B. J. Hunsinger and K. Hanma, US Patent No. 162465 (1979).
16. K. Yamanouchi and H. Furuyashiki, Electron. Lett. **20** (20), 819 (2007).
17. D. S. Ballantine, S. J. Martin and A. J. Ricco, *Acoustic Wave Sensors* (Academic Press, 1996).
18. I. Huang, J. Micro/Nanolithogr., MEMS, MOEMS **12** (1), 9303 (2013).
19. X. Ji, Y. Fan, T. Han, and P. Cai, Acoust. Phys. **62** (2), 160 (2016).
20. D. H. Wu and H. H. Chen, IEEE Trans. Ultrason., Ferroelectr. Freq. Control **52** (12), 2403 (2005).
21. I. Y. Huang, C. Y. Lin, and J. W. Lan, J. Micro/Nanolithogr., MEMS, MOEMS **12**, 013019 (2013).